Defence Science Journal, Vol. 71, No. 6, November 2021, pp. 737-747, DOI : 10.14429/dsj.71.15803

Impact and Ricochet of a High-speed Projectile from a Plate

Hussein Bassindowa[#], Bakhtier Farouk[#,*], and Steven B. Segletes[@]

[#]*Mechanical Engineering Department, Drexel University, Philadelphia PA 19104, United States*
[@]*Impact Physics, Army Research Laboratory, Aberdeen MD 21005-5425, United States*
[*]*E-mail: bfarouk@drexel.edu*

ABSTRACT

A computational study of a projectile (either 2024 *aluminum or* $TiAl_6V_4$ *titanium alloy*) impacting a plate (either *titanium alloy or aluminum*) is presented in this paper. Projectile velocity (ranging from 250 m/s to 1500 m/s) with varying impact angles are considered. The presence of ricochet (if any) is identified over the ranges of the projectile velocity and impact angle considered. For the cases where ricochet is identified, the ricochet angle and velocity are predicted as functions of the incident angle and the incident velocity. The numerical results are compared with an analytical solution of the ricochet problem. The analytical solutions are from a model developed to predict the ballistic ricochet of a projectile (projectile) penetrator. The dynamics and the deformation of an aluminum (or a titanium alloy) projectile impacting on a finite thickness titanium alloy (or aluminum) plate are simulated. The current work is interesting in that it looks in the field of ballistics of different material combinations than are traditionally studied. The present simulations based on detailed material models for the aluminum and the titanium alloy and the impact physics modelling features in the LS-DYNA code provide interesting details regarding the projectile/plate deformations and post-impact projectile shape and geometry. The present results indicate that for no cases (for specified incoming velocities and impact angles considered) can an aluminum projectile penetrate a titanium alloy plate. The ricochet 'mode predictions 'obtained from the present simulations agree well with the ricochet 'mode predictions' given in an analytical model.

Keywords: Ricochet; Plastic-hinge ricochet; Two-way contact treatment; Tabulated Johnson-Cook plasticity model

1. INTRODUCTION

The projectile shape, velocity, projectile material, spin, target material and the angle of incidence determine the possibility of ricochet[1]. Projectiles (say bullets) that break up have a low risk of ricochet. Projectiles easily ricochet off water[2]; as found in the stone skipping phenomenon in ponds and lakes.

In some instances, ricochets can cause the return of the projectile to the shooter[3]. In general, the ricochet process could be controlled by the shape, the size, the strength, the launching velocity, and the incident angle of the projectile as well as the mechanical properties of the target medium. In the past, research work has focused on the ricochet of projectiles off water surface and debris with different materials against soft ground.

Since ricochet related experiments (from a solid surface) are costly, time-consuming and limited in obtaining data - numerical simulation is an attractive alternative for studying the high-speed impact and ricochet phenomenon. In this paper, a numerical study on a projectile (2024 aluminum or $TiAl_6V_4$ titanium alloy) impacting a plate ($TiAl_6V_4$ titanium alloy or 2024 aluminum) is presented. In the current study, 3-D time-dependent numerical simulations were performed by using a general-purpose finite element program LS-DYNA[4] - capable of simulating complex real world problems. The code's origin lie in highly nonlinear, transient dynamic finite element analysis using explicit time integration. The purpose of the present simulations was to elucidate the rich physics in the impact of a soft (aluminum) / hard (titanium alloy) projectile impacting a hard (titanium alloy) /soft (aluminum) plate over a range of projectile velocity (V) and impact angle (θ).

Received : 08 May 2020, Revised : 07 April 2021
Accepted : 09 July 2021, Online published : 22 October 2021

2. REVIEW OF THE PAST WORK

When an object strikes the surface of a liquid medium, a lift reaction force capable of bouncing the object off the surface can be produced[5]. The effect of sea waves on a 0.50 caliber bullet ricocheting off sea water is reported[6]. In another study[7], experimental and FEM modelling was carried out to determine the temperature effect upon a sphere ricochet on sand. Park[8], *et al.* examined the physics of arbitrary-shaped bodies entering an air-water interface by employing the source panel numerical method. An early theory of ricochet from an air-water interface was proposed by Birkhoff[9], *et al.* The application of the theory is found in an interesting paper by Johnson and Reid[10]. The theory[8] predicts the required angle of attack at a liquid surface, θ_{cr} for a uniform solid sphere to exhibit ricochet. The observations show that the water pressure due to the impact must act over a considerably greater area than that assumed in Birkhoff[9], *et al.*. The effect of projectile spin was accounted for in theory proposed by Hutchings[11].

Hutchings also applied the Rayleigh formula[12] to a spherical projectile and to a spinning cylinder impacting an air-water interface. Farouk[13], *et al.* carried out a numerical study of ricochet of a rigid sphere off a water layer. The results were compared with available analytical solutions and experimental data of the problem.

In this study, a numerical study on a projectile (2024 aluminum or $TiAl_6V_4$ titanium alloy) impacting a plate (titanium alloy or aluminum) is presented. 3-D time-dependent numerical simulations were performed by using a finite element program LS-DYNA[4].

3. PROBLEM DESCRIPTION

The impact of an aluminum (or a titanium alloy) projectile of length 30.0 mm and diameter of 6.0 mm (with a 6.0 mm diameter spherical endcap) is considered for the present simulations. The high-velocity projectile impacts a titanium alloy (or an aluminum plate) having a length L_x = 130.0 mm, a width L_z = 120.0 mm and a thickness L_y = 10.0 mm (see Fig. 1, *not to scale*). The projectile (parallel to the x-y plane) is placed close to the plate about x = 30.0 mm from the left edge and along the middle of the width of the plate z = 60.0 mm with specified angle o inclination.

The following assumptions were made in the model development:

1. The air resistance to the projectile before, during and after the impact process is neglected. Such resistances are assumed to be negligible for the vases considered.
2. The SPC (single point constraint) boundary condition[14] is invoked along the four edges of the plate rendering the edges as clamped.
3. The resultant (initial) velocity of the projectile is parallel to the x-y plane with an obliquity angle θ with respect to the perpendicular, for all cases considered.

4. MATHEMATICAL MODEL OF IMPACT

The model geometry considered in the present study consists of two parts: the solid plate and the impacting solid (a hemispherical nose projectile). The two main methods for advection are the Van Leer and the 'donor cell' methods.

The following equation of motion is considered in this work for the impact simulation[14]:

$$ma + cv + f_{\text{int}} = f_{ext} \tag{1}$$

With m and c being the mass and the damping factor respectively; while a and v are the acceleration, and velocity vectors. Additionally, f_{ext} and f_{int} are the external and internal forces. The equation of motion is solved using the initial inputs (at t = 0) and the values are updated after subsequent time intervals. The internal forces are found by

$$f_{\text{int}}^{n+1} = \int_V B^T \zeta^{n+1} dV \tag{2}$$

where ζ is the stress on the element and it is updated along with the strain ε from the constitutive relations of the material, V is the volume (in this case it is the volume of the element), and B^T is the transpose matrix of the strain displacement matrix B. Finally, from body loads and material properties specified, the external forces f_{ext} are computed.

The energy equation[14]

$$\dot{E} = Vs_{ij}\dot{\varepsilon}_g - (p)\dot{V} \tag{3}$$

is integrated in time and is used for equation of state calculations and global energy balance. In the above equation, E is the total energy, $(dE = c_p dT$ where T is the temperature), s_{ij} and p represent the deviatoric stresses and pressure. Also, V is the relative volume, $\dot{\varepsilon}_q$ is the strain tensor and $\dot{V}$ is the rate of volume change.

Appropriate initial and boundary conditions are imposed for the numerical solution of the governing equations for the impact problem[15] shown schematically in Fig. 1 earlier. Further details of the mathematical model for the impact problems considered here can be found in the LS-DYNA theory manual [14].

5. NUMERICAL MODEL OF AN IMPACT

Various CONTACT keywords are available in LS-DYNA[14] for treating interactions between disjointed parts. A two-way contact treatment option *'eroding_surface_to_surface'* was applied in the simulations reported in this paper. This two-way contact option works essentially the same way as a one-way contact option except that the subroutines that check the slave (say plate) nodes for penetration, are called a second time to check the master (say projectile) nodes for penetration through the slave segments[14].

For the present simulations (employing LS-DYNA), the Material Type 224 (MAT_224: tabulated_Johnson_Cook)[16] was used to model both the 2024 aluminum and the titanium alloy ($TiAl_6V_4$). The reason for selecting these materials (MAT_224) is due to the availability of the necessary parameters (in LS-DYNA), needed to model the impact behaviour of these materials. Table 1 shows the properties used for the two metal (aluminum and titanium alloy) material models.

5.1 The Tabulated Johnson-Cook Material Model (MAT_224)

An elasto-visco-plastic material with arbitrary stress versus strain curves and arbitrary strain rate dependency can be characterised using the tabulated Johnson-Cook material model[14]. Pressure is calculated from the stress-strain tables

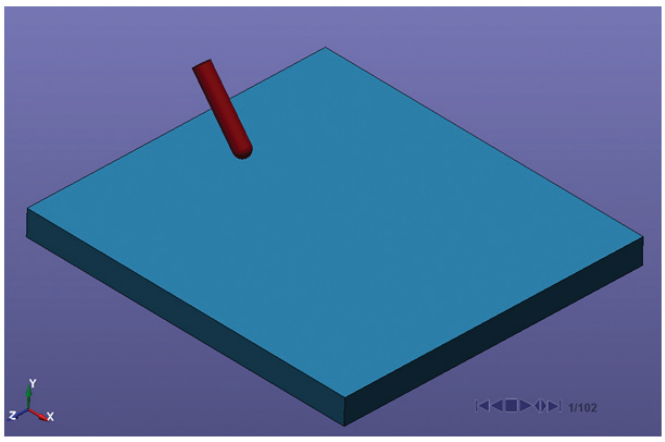

Figure 1. Problem geometry considered for the projectile ricochet problem (for the schematic, θ = 40°).

Table 1. Results for the cases considered of an aluminum projectile on a titanium alloy plate (Al/Ti) (Note: PH = plastic hinge, Pen = penetration, B/R = buckle/rebound, FS = flow split[17-19])

Case	Impact velocity (m/s)	Impact angle (θ)	Ricochet (Y/N) from the simulations	Ricochet angle (α) from simulations	Projectile status after impact	Ricochet mode from the analytical model	Ricochet angle (α) from the analytical model
1A (Base case)	250	15°	Y	28°	Bent Projectile	B/R	--
1B	250	30°	Y	20°	Bent Projectile	PH	0°
2A	500	25°	Y	36°	Hinge/Rebound w bent projectile and face eroded	FS	--
2B	500	40°	Y	27°	Hinge/Rebound w bent projectile and face eroded	PH	20°
2C	500	50°	Y	28°	Hinge / Rebound w bent projectile	PH	0°
3A	1000	30°	N	--	Shattering w tail part intact/ flattened	PH/FS	29°
3B	1000	45°	Y	0°	Shattered tip only w upper part and tail intact/flattened	PH	38°
3C	1000	60°	Y	10°	Slightly flattened and intact	PH	14°
4A	1500	30°	N	--	Shattered / small dent	FS	--
4B	1500	40°	N	--	Shattered/ small dent	FS	--
4C	1500	50°	N	--	Shattered/ small dent	FS	--
4D	1500	60°	Y	8°	Slightly flattened/intact	PH	24°

associated with MAT_224. Optional plastic failure strain ε_{pf} can be defined as a function of triaxiality (ratio of hydrostatic pressure or mean stress *p*, to the von Mises equivalent stress (σ_{vm}) $\frac{p}{\sigma_{vm}}$, the LODE parameter (normalised third stress invariant (J_3) $\frac{27J_3}{2\sigma_{vm}^3}$, the strain rate $\dot{\varepsilon}_P$, temperature T and the element size l_c (square root of element area for shells and volume over maximum area for solids) as shown in the following:

$$\varepsilon_{pf} = f\left(\frac{p}{\sigma_{vm}}, \frac{27J_3}{2\sigma_{vm}^3}\right) \cdot g\left(\dot{\varepsilon}_P\right) \cdot h(T) \cdot i\left(l_c, \frac{p}{\sigma_{vm}}\right) \quad (4)$$

The default failure criteria *F* below depends on the time accumulation of plastic strain rate $\dot{\varepsilon}_P$ and plastic failure strain ε_{pf}:

$$F = \int \frac{\dot{\varepsilon}_P}{\varepsilon_{pf}} dt \quad (5)$$

where failure occurs when $F \geq 1$.

5.2 Discretisation and Mesh Structure

Relatively fine finite element meshes were created for the plate (130 x 120 x 10) and the cylindrical projectile with a hemispherical head (~ 57000 elements) (see Fig. 1). For the impact velocity of the projectile varying between 250 m/s and 1500 m/s, the time step of 1.0 μs was used for the simulations. For all cases studied, the projectile was placed very close to the plate – so that the impact was almost immediate. Calculations with 10% higher mesh density for the plate and the projectile provided very similar results for the ricochet behaviour for the base case 1A (see Tables 2 and 3).

6. RESULTS AND DISCUSSION

6.1 List of Cases Simulated with Comparison of Results

A total of four different impact velocities of the projectile are considered for two sets of cases for the simulations at varying impact angles as shown in Tables 1 and 2 below. The first set of cases (Table 1) considers an aluminum projectile impacting a titanium alloy plate, labelled as (Al/Ti), and then reversing the materials for the second set (Table 2), labelled as (Ti/Al). All velocities and impacting angles considered are kept the same for the two combinations considered. The significant results from the simulations are also shown in Tables 1 and 2 below. The last column in the two tables provide summary observations from the simulations carried out that indicates the projectile status after impact.

Cases 1A and 1B (in both tables) consider impact angles of θ= 15° and 30° respectively. The impact velocity is 500 m/s in cases 2A thru 2C at impact angles θ= 25° 40° and 50° respectively. Cases 3A thru 3C consider an impact velocity of 1000 m/s at impact angles θ= 30° 45° and 60° respectively. An impact velocity of 1500 m/s is considered in cases 4A through 4D at impact angles θ= 30°, 40°, 50° and 60° respectively. The impact (θ) angle is measured from the horizontal x and the ricochet (α) angle is measured from the vertical axis (see Fig. 1). Tables 1 and 2 also summarise the main results from the simulations indicating whether ricochet was observed or not, and the projectile physical status after the impact. The last two columns in the two tables list the results/observations from the analytical models of Segletes[17-19].

The ricochet angles (if any - shown in Tables 1 and 2, column 5) are calculated from the x-y location of the center-of-gravity of the projectile after the ricochet. In column 6,

Table 2. Results for the cases considered of a titanium alloy projectile on an aluminum plate (Ti/Al) (Note: PH = plastic hinge, Pen = penetration, B/R = buckle/rebound, FS = flow split[17-19])

Case	Impact velocity (m/s)	Impact angle (θ)	Ricochet (Y/N) from the simulations	Ricochet angle (α) from simulations	Projectile status after impact	Ricochet mode from the analytical model	Ricochet angle (α) from the analytical model
1A Base case	250	15°	N	--	Projectile reflected	PH or B/R	--
1B	250	30°	Y	66°	Bent projectile	PH	0°
2A	500	25°	N	--	Projectile embedded	PH	13°
2B	500	40°	Y	37°	Hinge / bent rebound projectile	PH	0°
2C	500	50°	Y	18°	Hinge / bent rebound projectile	PH	0°
3A	1000	30°	N	--	Perforate /projectile face damage	Pen	---
3B	1000	45°	N	--	Perforate/projectile face damage	Pen	---
3C	1000	60°	Y	30°	Hinge / rebound	PH	0°
4A	1500	30°	N	--	Perforate /projectile face damage	Pen	--
4B	1500	40°	N	--	Perforate /projectile face damage	Pen	--
4C	1500	50°	N	--	Perforate/projectile face damage	Pen	--
4D	1500	60°	Y	27°	Hinge / Rebound	Pen	--

Table 3. Material parameters for a 6 mm diameter projectile against a finite 10 mm thick plate, drawn largely from[22,23]

Property	Aluminum 2024	Titanium alloy $TiAl_6V_4$
As projectile (rod)		
Mass density ρ kg/m^3	2.78 x 10^3	4.43 x 10^3
Tensile yield strength *Y* GPa	0.324	0.880
As plate (target)		
Ultimate strength σ ult GPA	0.469	0.950
Elastic modulus *E* GPA	73.1	113.8
$H_{semi\text{-}infinite}$ GPa	2.490	4.7945
α	7	7
Poisson's ratiov	0.330	0.342
Ballistic resistance *H* GPa	1.876	3.613
$V_{B/R}$ m/s	< 630	< 483
V_{FS} m/s	< 673	< 1538

the projectile status (from the simulations) is listed. From the analytical model (details to follow), the ricochet mode (PH = plastic hinge, P_{en} = penetration, B/R = buckle/rebound, or FS = flow split)[15-17] is ascertained for each case (in column 7). Flow splitting is a situation where the impact speed is too low for penetration, and the obliquity too small to sustain a plastic hinge. In this case, the projectile tends to flatten (i.e., mushroom or, in an extreme case, pancake) upon the target surface, until its inertia is expended. In the very last column, the ricochet angles predicted by the analytical model[18] are shown.

6.2 Impact Simulation Results with Projectile and Target Status

Figures 2 and 3 below show the instantaneous projectile shape and position at three impact angles (15°, and 30°) considered.

For the case 1A shown in Fig. 2(a), the rounded head of the aluminum projectile undergoes considerable plastic deformation (bending) and assumes a flat-head type shape. The rebound angle (α) is approximated to be around 28° (with α>θ). While the case in Fig. 2(b) shows the titanium projectile reflecting (bouncing back) instead of ricocheting off the plate.

The tendency of the analytical model to predict plastic-hinge ricochet at these slow velocities arises because (being designed for ballistic velocity engagements) the analytical ricochet model does not account for deceleration of the rod. Thus, in the actual case, where the impact momentum is depleted in the initial stages of rod/target contact, the analytical

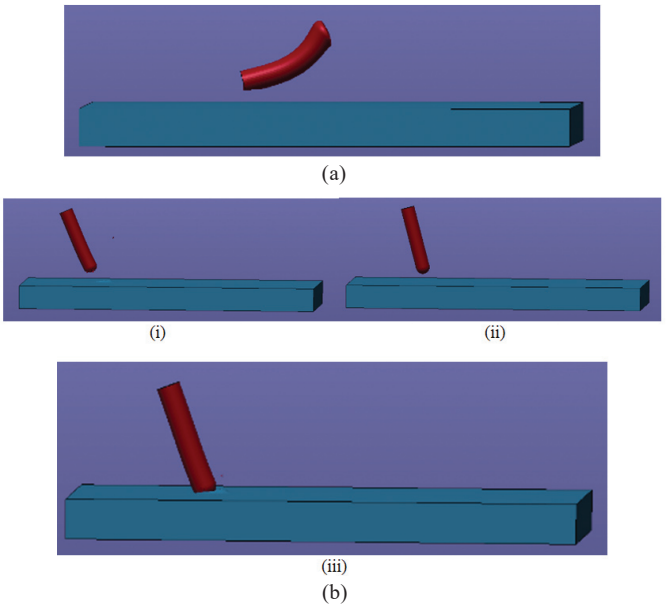

Figure 2. Projectile shape and orientation after impact for case 1A (impact velocity: 250 m/s; impact angle: 15°): (a) (Al/Ti) at t = 0.4 ms and (b) (Ti/Al) at: (i) t= 0.004 ms; (ii) t=0.15 ms; (iii) t =0.4 ms.

model fails to capture the deceleration that prevents a plastic hinge from forming. Of course, whether the projectile response at low impact velocity is buckle/rebound (B/R) or plastic-hinge ricochet (PH), the net effect is that the projectile is bent and deflected from an essentially undamaged target.

For the Case 1B where the aluminum projectile hits the plate at θ = 30° (Fig. 3(a)), the projectile departs with a shallower rebound angle (~ 20°) compared to the case where θ = 15° and tip is almost as deformed (bent) as the shape shown in Fig. 2(a). As for the case in Fig. 3(b), the titanium projectile rebounds off the aluminum plate with less deformation than the aluminum case but with higher departure angle as well. The simulations for this low velocity case are found to predict higher rebound angle compared to the analytical model predictions[18].

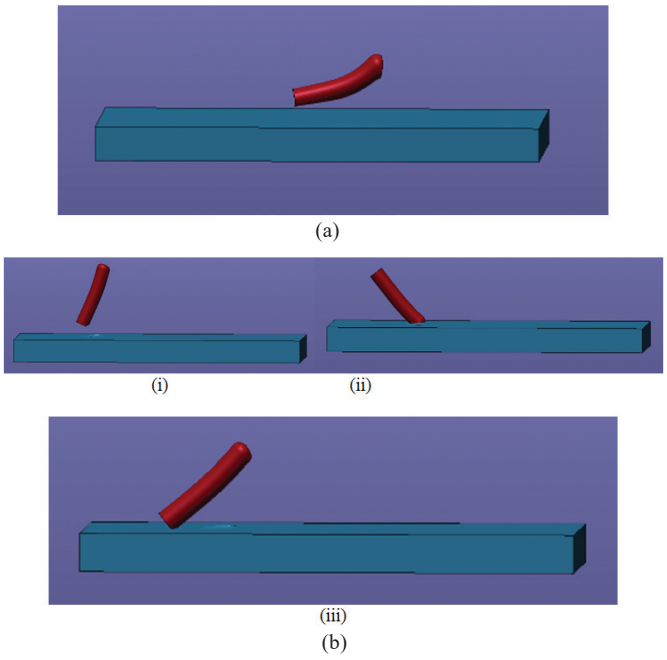

Figure 3. Projectile shape and orientation after impact followed by ricochet for case 1B (impact velocity: 250 m/s; impact angle: 30°): (a) (Al/Ti) at t = 0.4 ms and (b) (Ti/Al) at: (i) t= 0.05 ms; (ii) t=0.28 ms and (iii) t =0.4 ms.

Figures 4 below show the instantaneous projectile shape and position for the impact velocity of 500 m/s at the impact angles 25° considered: cases 2A in Table 2. It is shown that the plastic deformation on the shape of the projectile is more dramatic in case 2A, with the face of the projectile being eroded in some cases.

Figures 4(a) and 4(b) show the instantaneous location and shape of the projectile with θ = 25° for both cases (Al/Ti) and (Ti/Al), the contours of the instantaneous von Mises (effective stress) are shown, as well.

The results shown in Figs. 5 and 6 (impact velocity of 500 m/s, with θ = 40° and 50°, cases 2B and 2C respectively) are similar with the projectile undergoing ricochet with plastic-hinge for both sets. The dynamic nature of the impact is clearly demonstrated by the stress field. The ricochet angle for case 2B shown in Fig. 5(a) is found to be about 37° from the simulations. Figure 5(b) shows that the titanium projectile

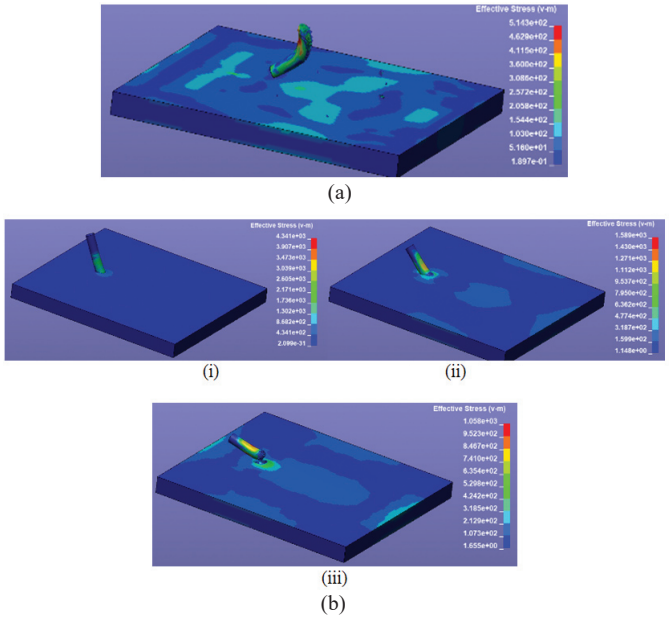

Figure 4. Contours of effective stress (Von-Mises) levels after impact, Case 2A(impact velocity: 500 m/s; impact angle: 25°): (a) (Al/Ti) t = 0.016 ms; min 0.019 MPa; max 514.0 MPa and (b) (Ti/Al) at: (i) t = 0.018 ms; min 0.0 MPa; max 4341.0 MPa; (ii) t = 0.088 ms; min 1.15 MPa; max 1589.0 MPa; (iii) t = 0.18 ms; min 1.66 MPa; max 1058.0 MPa.

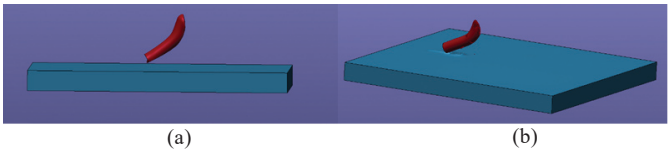

Figure 5. Projectile shape and orientation after impact followed by ricochet, case 2B (impact velocity: 500 m/s; impact angle: 40°) at t = 0.16 ms (a) (Al/Ti) and (b) (Ti/Al).

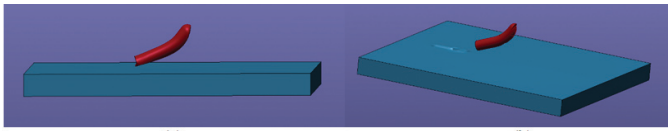

Figure 6. Projectile shape and orientation after impact followed by ricochet Case 2C (impact velocity: 500 m/s; impact angle: 50°) at t = 0.16 ms (a) (Al/Ti) and (b) (Ti/Al).

was first embedded in the plate before being ejected from its surface without ricochet.

Figures 7 below show the instantaneous projectile shape and position for the impact velocity of 1000 m/s at the impact angle of 30° considered (case 3A in Tables 2 and 3).

The impact in case 3A (aluminum projectile, titanium alloy plate) is characterised by 'flow-split' (FS) as shown in Fig. 7(a) for an impact angle θ = 30°. The aluminum projectile fractures into multiple pieces as it goes through the plastic deformation. While Fig. 7(b) shows the titanium projectile penetrating through the aluminum plate with the head of the projectile partially disintegrated.

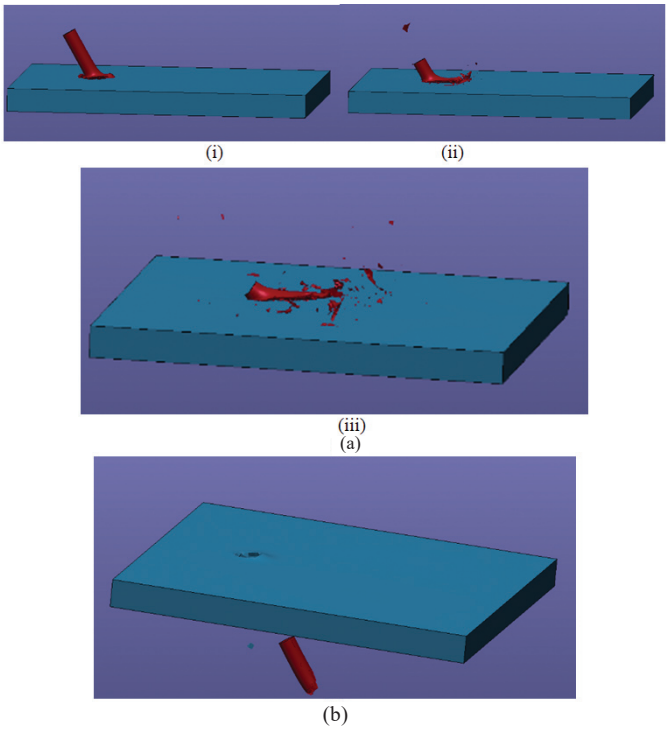

Figure 7. Projectile shape and orientation after impact, case 3A, No-Ricochet, (impact velocity: 1000 m/s; impact angle: 30°) (a) (Al/Ti) at (i) t = 0.012 ms; (ii) t=0.026 ms; (iii) t=0.06 ms and (b) (Ti/Al) at t= 0.09 ms "penetration".

The impact for cases 3B (Al/Ti) could be characterised as either plastic-hinge ricochet or flow split as shown in Fig. 8(a) for an impact obliquity of θ = 45°. We will choose to call it ricochet, as the top surface of the projectile remains largely intact and there is negligible lateral spread of what little projectile (rod) debris that is produced. Nonetheless, the aluminum projectile-head fractures into two pieces while the rest of the projectile body is somewhat intact.

The above simulation (Fig. 8(a)) indicates the leading-edge piece to have a ricochet angle of about 4°, compared to the analytical model prediction of 29°. Case 3B (Ti/Al, Fig. 8(b)) shows penetration similar to what is seen in case 3A (Ti/Al, Fig. 7(b)).

The projectile is found to ricochet (in one piece) for θ = 60° (Case 3C) as shown in the first set ((Al/Ti), Fig. 9(a)) below, while for the second set ((Ti/Al), Fig. 9(b)) the titanium projectile is also seen ricocheting off the aluminum plate albeit with a rather large gouge on the surface.

Figures 10-13 below show the instantaneous projectile shape and position for the impact velocity of 1500 m/s at the four impact angles (30°, 40°, 50° and 60°) considered for cases 4A – 4D for both sets. The first set for case 4A (Al/Ti, Fig.10(a)) where the projectile, characterised by a flow split, is shattered upon impact but due to the acute angle and high speed, it leaves an impression on the plate. Whereas for the second set (Ti/Al), Fig. 10(b)) the projectile penetrates the plate.

The results for case 4B are shown in Fig. 11. Again, the first set (Al/Ti, Fig. 11(a)) is characterised by 'flow-split' (FS) below for an impact angle θ = 40°. The projectile fractures into

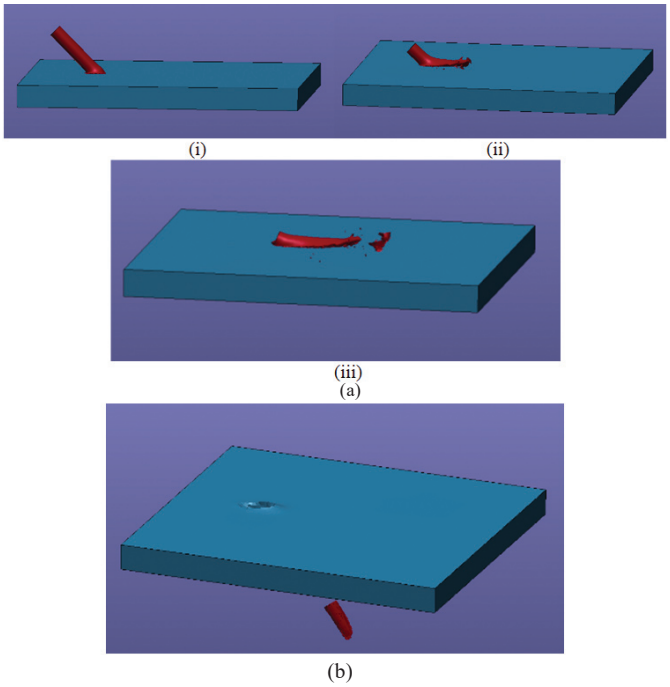

Figure 8. Projectile shape and orientation after impact, case 3B, 'penetration' (impact velocity: 1000 m/s; impact angle: 45°): (a) (Al/Ti) at (i) t = 0.008 ms; (ii) t=0.026 ms; (iii) t=0.062 ms and (b) (Ti/Al) at t=0.13 ms "penetration".

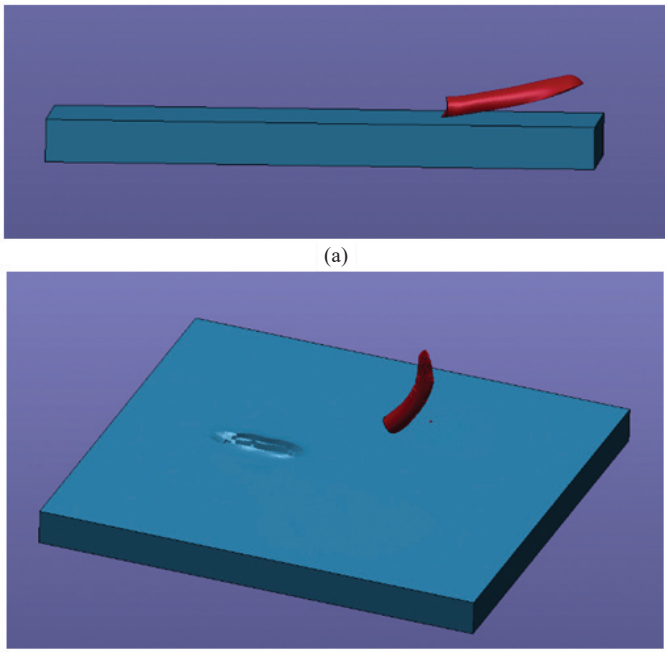

Figure 9. Projectile shape and orientation after impact followed by ricochet, case 3C, Ricochet, (impact velocity: 1000 m/s; impact angle: 60°): (a) (Al/Ti) at t = 0.1 ms and (b) (Ti/Al) at t = 0.12 ms.

multiple pieces and it leaves a smaller impression than what was observed in first set of case 4A shown in Figs. 10(a) and 10(b). The second set (Ti/Al, Fig. 11(b)) shows the projectile going through the plate as seen in Fig.10(b).

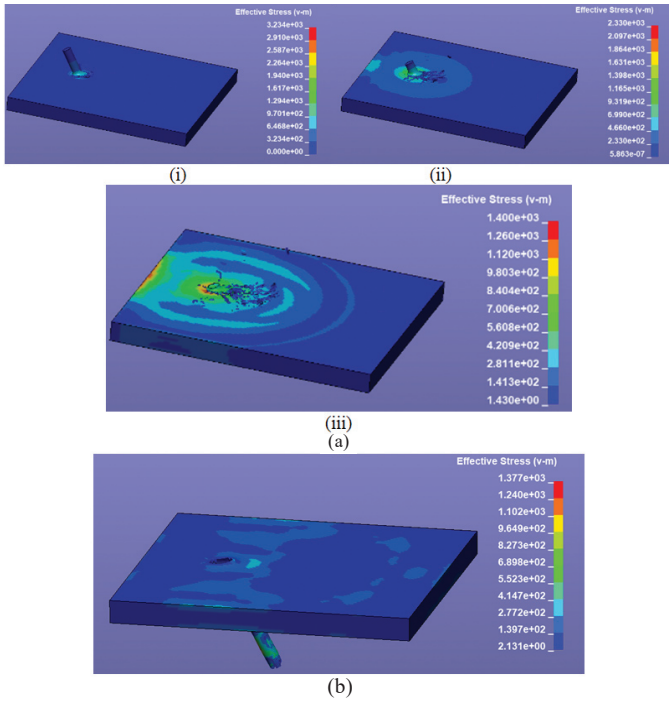

Figure 10. Contours of effective stress (Von-Mises) levels after impact "no ricochet", case 4A (impact velocity: 1500 m/s; impact angle: 30°): (a) (Al/Ti) at (i) t = 0.01 ms min 0 MPa; max 3242.0 MPa; (ii) t= 0.018 ms min 0.0 MPa; max 2330.0 MPa; (iii) t= 0.026 ms min 1.430 MPa; max 1400.0 MPa and (b) (Ti/Al) at t= 0.05 ms, min 2.131 MPa; max 1377.0 MPa "penetration".

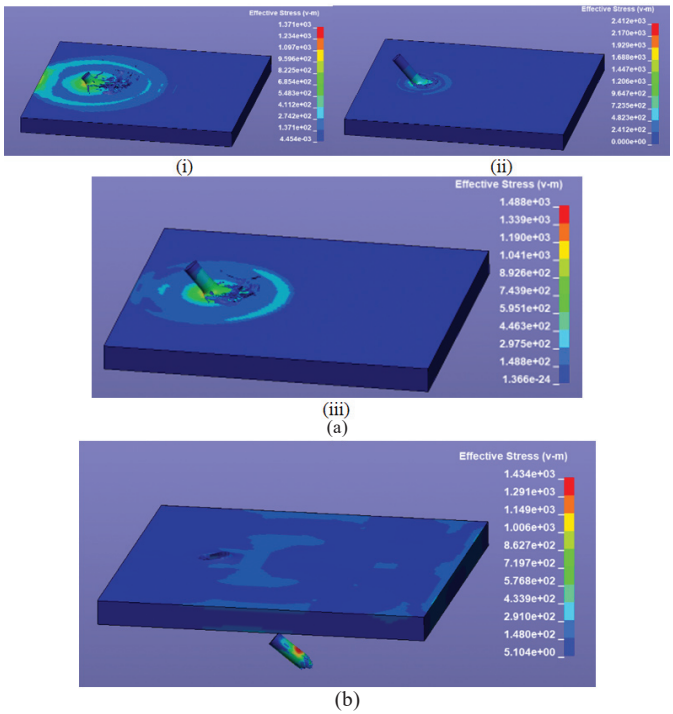

Figure 11. Contours of effective stress (Von-Mises) levels after impact "No ricochet", case 4B (impact velocity: 1500 m/s; impact angle: 40°): (a) (Al/Ti) at (i) t = 0.01 ms min 0 MPa; max 2412.0 MPa; (ii) t= 0.014 ms min 0.0 MPa; max 1448.0 MPa; (iii) t= 0.02 ms min 0.004 MPa; max 1371.0 MPa and (b) (Ti/Al) at t= 0.058 ms min 5.10 MPa; max 1434.0 MPa "Penetration".

The results (Al/Ti) for cases 4C (impact velocity of 1500 m/s) are characterised by flow split (FS), as shown in Fig. 12(a) below for impact angles of θ = 50°.

The results (Al/Ti) for cases 4D (impact velocity of 1500 m/s) are characterised by a plastic hinge (PH), as shown in Fig. 13(a) below for impact angles of θ = 60°.

The aluminum projectile shatters upon impact for case 4C (Al/Ti) for θ = 50° (Fig. 12(a)). The aluminum projectile is flattened while still intact for θ = 60° as shown in Fig. 13(a) above. Here also the analytical model[18] predicts a higher ricochet angle than that predicted from the simulations. As for the second set (Ti/Al) for case 4C, (Fig. 12(b)), the projectile again penetrates the plate at the impact angle θ = 50°. However, case 4D shows that for an impact angle θ = 60°, the titanium alloy projectile ricochets off the plate with a large dent on the aluminum plate as shown in Fig. 13(b).

For the present simulations, the projectile and the plate are considered to be initially at a uniform temperature (298 K). We consider the energy equation in our LS-DYNA simulations; however, no noticeable temperature rise is observed either in the projectile or the plate as the contact between them lasts for very short times (of the order of micro-second).

To summarise, a total of four different impact velocities of the projectile are considered for two sets of cases for the simulations at varying impact angles as shown in Tables 1 and

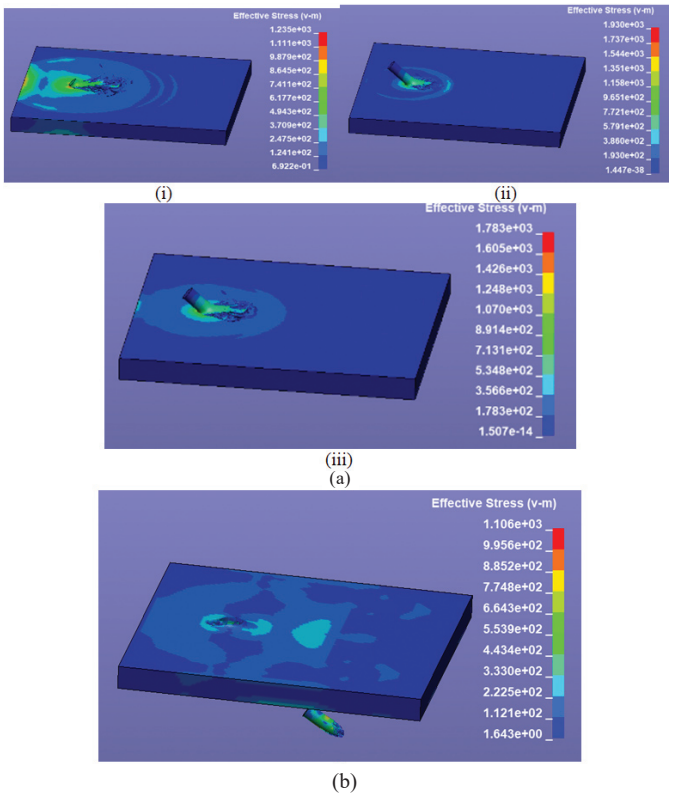

Figure 12. Contours of effective stress (Von-Mises) levels after impact "No ricochet", case 4C (impact velocity: 1500 m/s; impact angle: 50°): (a) (Al/Ti) at (i) t = 0.012 ms min 0 MPa; max 1930.0 MPa; (ii) t= 0.016 ms min 0.0 MPa; max 1783.0 MPa; (iii) t= 0.024 ms min 0.69 MPa; max 1235.0 MPa and (b) (Ti/Al) at t= 0.067 ms min 1643.0 MPa; max 1106.0 MPa "penetration".

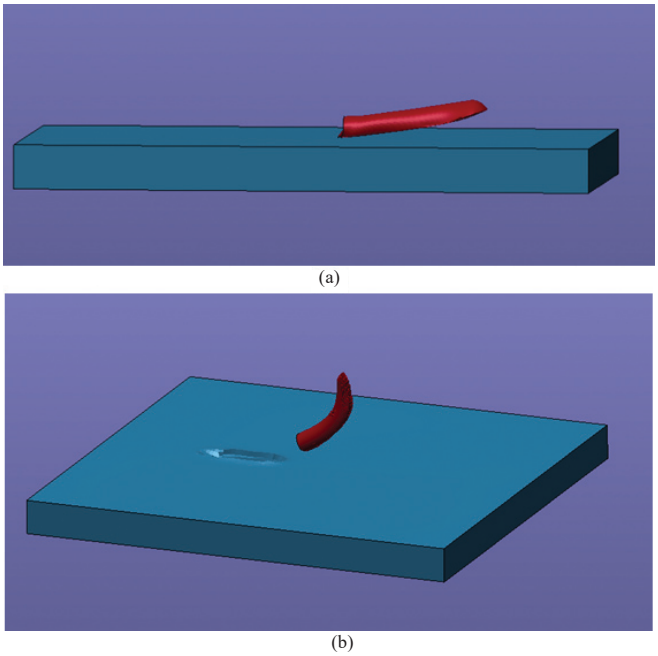

Figure 13. Projectile shape and orientation after impact followed by ricochet, case 4D (impact velocity: 1500 m/s; impact angle: 60°) at t = 0.084 ms: (a) (Al/Ti) and (b) (Ti/Al).

2 presented earlier. The last column in the two tables provide summary observations from the simulations carried out that indicates the projectile status after impact. Tables 1 and 2 also summarise the main results from the simulations indicating whether ricochet was observed or not, and the projectile physical status after the impact. In column 6, the projectile status (from the simulations) is listed. From the analytical model (details to follow), the ricochet mode (PH = plastic hinge, P_{en} = penetration, B/R = buckle/rebound, or FS = flow split)[15-17] is ascertained for each case (in column 7).

The material properties of 2024 aluminum and titanium alloy $TiAl_6V_4$ used here are listed in Table 1 shown earlier. Generally, the broad range of titanium alloys are stronger than the numerous aluminum alloys, but there is overlap. Roughly speaking, aluminum and its alloys have a tensile strength range of 90 MPA to 570 MPa. Titanium and its alloys tend to cover the range of 172 MPa to 1,600 MPa. At the low end, commercially pure titanium grades are well below common "aerospace grade" aluminum alloys, but some widely used titanium alloys are stronger than any aluminum alloy. The present ricochet results reflect the consequences of the above properties, as we find the aluminum projectiles could not penetrate the titanium plate for the impact velocity (V) and impact angle (θ) ranges considered.

6.3 Comparison of the Present Results with an Analytical Solution[18]

A model to predict the ballistic ricochet of projectile penetrators was developed earlier[17-19]. The underlying phenomenology of ricochet is one where the impacting projectile feeds into *a plastic hinge* located at the projectile/target interface and is thus diverted from a penetrating trajectory.

The full form of the analytical model[18] arises from the simultaneous solution of a series of six algebraic equations that constitute the momentum-flux/force and moment balances upon the *plastic hinge*, subject to various material and kinematic constraints. The simple form of the model[19], dispenses with the moment balance and makes several simplifying kinematic assumptions that permit the ricochet criterion to be expressed as a closed form inequality. Compared against 24 ballistic tests, the Segletes models (in both forms) show an ability to predict the ballistic ricochet of an impacting projectile.

The analytical model[18] assumptions are discussed below:

(a) Material parameters employed by the analytical model are the projectile's density (ρ) and tensile yield strength (Y), as well as a parameter known in the ballistic community as the target resistance (H).

(b) The target resistance represents a scalar stress that a target may apply to an indenting rod, which derives from a full multi-axial target response. The analysis starts with the baseline value of target resistance proposed by Tate[20]:

$$H_{semi\text{-}infinte} = \sigma_{ult}\left[\frac{2}{3}+\ln\left(\frac{2E}{3\sigma_{ult}}\right)\right] \quad (6)$$

where σ_{ult} is the target material's ultimate strength, and E is the elastic modulus of the target material. The value of $H_{\text{semi}-\text{infinite}}$ represents the stress that a full half-space of target material is able to apply to a striking rod, to resist indentation and penetration. In practice, if the target thickness is finite, the effective target resistance, which we are calling H, is reduced from the semi-infinite value by

$$\frac{H}{H_{semi\text{-}\inf int\, e}} = \begin{cases} \dfrac{\ln(T/R+1)}{\ln\,\alpha} & (when\ T/R+1<\alpha) \\ 1 & (when\ T/R+1\geq\alpha) \end{cases} \quad (7)$$

here, T is the target thickness, R the projectile radius, and α a semi-empirical parameter[21] representing the extent of target plasticity relative to the indentation or crater radius. Other than α, which has been taken at a value of 7, all other parameters for our two materials of interest, 2024 Al and$TiAl_6V_4$, are taken from the ASM website[3,4], or calculated from the above equations and those which follow, as shown in Table 3.With these parameters input to the analytical model, the parameter space of impact velocity may be explored to find at which obliquities ricochet may occur.

In the ricochet regime, while both configurations reveal similar shape characteristics, the height (or thickness) of the α, η> 0 bands are larger for the aluminum projectile against the titanium target. When η > 0, the target is stressed to its material limit, even to the point of deforming to accommodate the line-of-force changes necessary to sustain ricochet. A stronger target, therefore, is more likely to sustain a wider band of η > 0 solutions, as we see here for the titanium target vis-à-vis aluminum. The projectile is always stressed to its yield limit during a ricochet event, or the plastic hinge could not form. In the α > 0 regime, however, that yielding is essentially brought about by compressive forces. Once ricochet reaches the α = 0 regime, the proportion of compression is reduced while

that due to pure bending is increased. The weaker aluminum projectile is capable of generating less axial force than the stronger titanium rod. Thus, a larger change in obliquity angle is generally required to reach α = 0 for the weaker projectile material, since a larger obliquity is needed to reduce the axial-force requirements for turning the projectile from its original trajectory.

For obliquity angles below the critical angle of ricochet, the velocity of the striking penetrator will determine what happens. The following statements apply to material combinations for which (H–Y)>Y which is true for both ballistic cases considered here. When the stagnation pressure of impact falls below the yield strength of the rod, buckling or rebound (B/R) will occur. The condition may be characterised by

$$V_{B/R} < \sqrt{\frac{Y}{0.5\rho}} \tag{8}$$

Beyond that velocity, and up to the point where the impact stress $(0.5V^2 + Y)$ exceeds target resistance H, flow splitting (FS) will occur, wherein the projectile "mushrooms" upon the surface of the target. This condition may be characterised by

$$V_{B/R} < V_{FS} < \sqrt{\frac{(H-Y)}{0.5\rho}} \tag{9}$$

Beyond the limit of flow splitting (and below the critical ricochet angle), true penetration (Pen) will occur, in which both the projectile (rod) and the target deform and erode in the process of forming a deformation crater within the target.

The line-of-force angle η has an influence on the value of α, the ricochet angle from the target surface. In the experimental data analysed by Segletes[18,19], the materials and velocity of the engagements were such that, if ricochet conditions were not met, the event transitioned to a penetration event. Distinguishing a ricochet from penetration is straightforward, in such a case.

From the present simulation results, a different regime of ricochet is also explored, in which the target (plate) is not always expected (or barely so) to become plastic. The present LS-DYNA simulation results are compared with the above analytical model[17-19] below. This complicates the theoretical analysis[18] somewhat, since a non-ricochet event can become, instead, a 'deform-and-rebound' event. Figures 14(a) and 14(b) show the predictions of the ricochet phenomena (from Tables 2 and 3) for both simulation sets, indicated by symbols in the V-θ plane. The regions η > 0, α > 0 and α = 0 all correspond to regions of plastic-hinge ricochet. The ricochet modes are identified as PH = plastic hinge, Pen = penetration, B/R = buckle/rebound, and FS = flow split in[18]. In general, the ricochet 'mode predictions' from the simulations agree very well with the ricochet 'mode predictions 'from the analytical model - based on the impact velocity (V) and the impact angle (θ).

In Fig. 14(a), representing the (Al/Ti) series, at the 250 m/s impact speed, the 30° obliquity simulation (case 1B) reported a rebound, rather than a plastic hinge. We believe this discrepancy arises from the inability of the analytical model to account for projectile deceleration, which is more decisive at lower impact speeds.

To explain the comparisons shown in Fig. 14(a). at 500 m/s, 25° (case 2A, Fig. 3(a)), the analytical prediction placed the behaviour on the boundary of buckle/rebound and flow splitting; however, the simulation seemed to indicate the formation of a plastic hinge. However, in the simulation, the hinge was unable to sustain itself because of projectile deceleration, and the hinge ricochet eventually transitioned into a rebound event. At 1000 m/s, 30° (case 3A), the analytical model placed the behaviour on the boundary of flow splitting and plastic hinge formation. The corresponding simulation revealed flow splitting. In all other (Al/Ti) cases, the simulations agreed with the results of the analytical model.

Figure 14(b) above represents the simulation comparison for the (Ti/Al) series of simulations. As with the (Al/Ti) series, the analytical predictions at 250 m/s (cases 1A and 1B) predicted ricochet where rebound was computationally observed. In the case of the 500 m/s, 25° case 2A simulation, the analytical model predicts a result with an η>0 plastic hinge, though the result lies near the region of rebound prediction. The simulation showed rebound. The high velocity, high obliquity simulation 4D was predicted by the analytical model

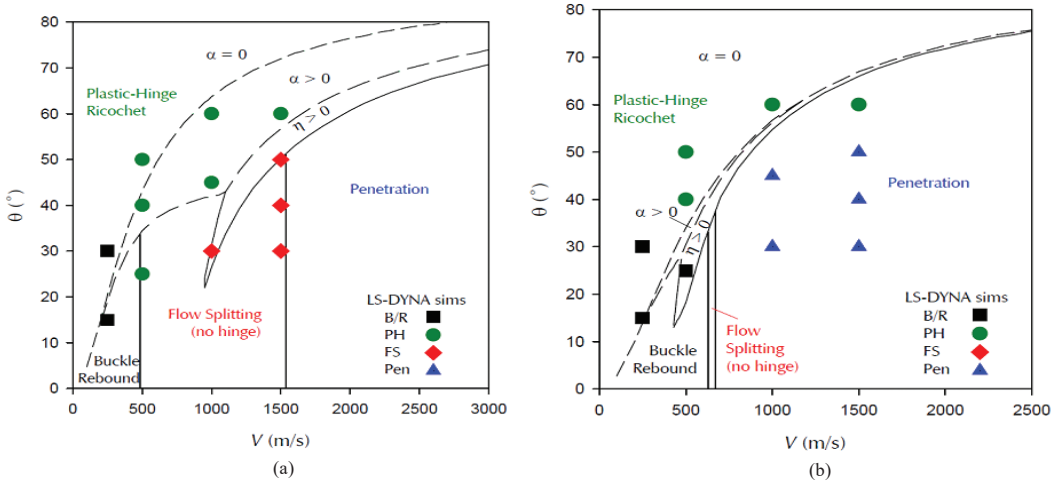

Figure 14. Depiction of the (V, θ) space explored via the simulations: (a) for the first set (Al/Ti), initial conditions denoted with symbols (symbol shape/colour denotes present simulation results) and (b) for the second set (Ti/Al), initial conditions denoted with symbols (symbol shape/colour denotes present simulation results).

to result in penetration; however, the simulation showed a "gouging ricochet." It has been mentioned that the analytical model is not able to account for these “gouging” type of ricochets, which perhaps explains the discrepancy. In all other (Ti/Al)cases, the simulations agreed well with the results of the analytical model.

6.3.1 Discussion

In the analytical model, the value of α (ricochet angle –measured from the horizontal *x* axis) may never exceed θ (impact angle – measured from the vertical y axis) during ricochet. For that to be violated would imply that the plastic hinge turns the projectile (rod) in excess of 90°, which is kinematically less preferable to penetration or rebound (and is thus excluded from viable plastic-hinge ricochets). In examining the details of predicted rebound angle α as a function of the impact obliquity θ, one will not find the plastic-hinge ricochet curves in the region $\alpha > \theta$.

The presence of target (plate) deformation allows the target-force line of action, η, to depart from the target normal which can also facilitate ricochet while concomitantly lowering the rebound angle α. Both analytical solution and the simulation agree that, at 1500 m/s impact speed, an obliquity of 30 degrees should result in penetration (see Fig. 9). Both the simulation at 1500 m/s, 60° obliquity (Fig. 12) and the analytical result indicate plastic-hinge ricochet, but a large disparity in the ricochet angle α is observed. While the analytical solution predicted a ricochet angle of 24.5°, the simulation produced a ricochet nearly parallel with the target surface ($\alpha \sim 0$ degrees).

At 1500 m/s, ricochet occurs between 50° and 60° degrees (Figs. 11 and 12) which is approximately predicted by the analytical model. Below 1500 m/s, penetration is not possible for aluminum into titanium according to the analytical model[18], confirmed by computations. At 1000 m/s, plastic-hinge ricochet at 45° and 60° predicted by the simulations also confirms the model. For titanium against aluminum targets, the ricochet at 1000 m/s is not seen until 60° obliquity, again confirmed by the analytical model. At 1000 m/s, for aluminum projectiles into titanium, (violent) flow-splitting (pancaking) seems to occur at 30° (the time-dependent simulations indicate impending ricochet for the projectile, which is not able to kinematically remain in a single full-length piece). The analytical model for this case is likewise at the borderline between a flow-splitting and plastic-hinge ricochet condition.

At 500 m/s and below, the analytical model still predicts formation of a plastic-hinge for ricochet. However, there does not seem to be enough inertia to sustain a plastic hinge, even if it wants to form, because of axial deceleration (which is not accounted for by analytical model). Thus, it is more difficult to draw comparison between the simulations and the analytical model predictions, though trends are not wholly incompatible with model. Plastic-hinge ricochet in simulations is generally at very shallow angle, significantly less than the $\alpha > 0$ ricochet angles predicted by analytical model. Through-thickness deformation (plastic work) of the projectile consumes significant kinetic energy in the simulations. This physics is not considered in the analytical solutions[18].

To summarise, the simulated results are compared by mapping them in a V-θ plane with defined zones from the analytical model (for the type of resulting ricochet) in Figs. 14(a) and 14(b). From the mapping of our predicted results (type of ricochet) in a V-θ plane with defined zones from the analytical model, excellent agreements are observed in most cases.

In the course of this investigation, an additional limitation was discovered on the analytical ricochet model[18] being used for comparison to the simulation results. The analytical model does not account for the axial deceleration of the projectile, but rather uses the initial velocity conditions to predict the viability of sustaining a plastic hinge. For very slow impacts (500 m/s impact speeds or less), the relative closing velocity of projectile and target did not remain at its original value through the course of the impact. This makes a direct comparison between model and simulation problematic at low impact speeds.

7. CONCLUSIONS

The ricochet of an aluminum/titanium alloy projectile from a titanium alloy/aluminum plate was investigated numerically. The results explain the complex dynamic processes and material deformations involved.

The following conclusions are drawn from the results presented above:

1. The dynamics and the deformation of an aluminum (or a titanium alloy) projectile impacting on a finite thickness titanium alloy (or aluminum plate) are simulated.
2. The impact angle and the impact velocity of the incoming projectile were systematically varied to investigate the resulting ricochet or non-ricochet behaviour.
3. The titanium alloy plate is a harder material for the aluminum projectile to penetrate than the aluminum plate for the titanium alloy projectile.
4. In no cases (for the specified incoming velocities and impact angles considered) can an aluminum projectile penetrate the titanium alloy plate.
5. An analytical model[17-19] predicts trends but can be significantly off from the present simulations in quantitative values of ricochet angle.
6. The analytical model predicts the critical angle of ricochet, with a few exceptions: a) very low velocities where projectile deceleration occurs before plastic-hinge ricochet can establish itself; and b) situations where gouging ricochet is shown to occur, in which an initially penetrating rod, is successively reoriented to an aspect conducive to ricochet.
7. The analytical model differentiates the non-ricochet conditions of bounce/rebound, flow splitting, and penetration.
8. The current work is interesting in that it looks in the field of ballistics of different material combinations than are traditionally studied.

Future experimental studies are recommended for further validation of the present simulations of ricochet of an aluminum projectile from a plate. Future simulation studies are also recommended for the ricochet of harder projectiles from softer targets like aluminum and composites.

REFERENCES

1. Burke, T. W. & Rowe, W. F. Bullet ricochet: acomprehensive review. *J. Forensic Sci.,* 1992, **37**, 1254-60. doi: 10.1520/JFS13312J
2. Nennstiel, R. Study of bullet ricochet on a water surface. *AFTE J.,* 1984, **16**, 88-93.
3. Joosten K. U. A case of "boomerang" bullet ricochet. *Int. J. Legal Medicine.* 2001, **115**, 70-1. doi: 10.1007/s004140000148
4. LSTC. LS-DYNA Keyword Users Manual, Version 971, Livermore Software Technology Corporation, Livermore CA. 2007.
5. Podesta, M. Bouncing steel balls on water. *Physics Education*. 2007, **42**(5), 466-479. doi: 10.1088/0031-9120/42/5/003
6. Mirshak, R. & Beech, T. Estimating ricochet hazard zones at sea. *J. Def. Modeling Simulation: Appl., Methodol., Technol*., 2018, **15**, 399-413. doi: 10.1177/1548512918771769
7. Kim, Y. K. & Choi, W. C. Ricochet of spheres on sand of various temperature. *Def. Sci. J*., 2018, **68**(2), 150-158. doi: 10.14429/dsj.68.11846
8. Park, M.-S.; Jung, Y.-R. & Park, W.-G. Numerical study of impact force and ricochet behavior of high speed water-entry bodies. *Comput. Fluids*., 2003, **32**, 939-51. doi: 10.1016/S0045-7930(02)00087-7
9. Birkhoff, G.; Birkhoff, G. D.; Bleick, W. E.; Handler, E. H.; Murnaghan, D. & Smith, T. L. Ricochet off water. AMP Memo No. 42.4M, 1944.
10. Johnson, W. & Reid, S. R. Ricochet of spheres off water. *J. Mech. Eng. Sci*., 1975, **17**, 71-81. doi: 10.1243/JMES_JOUR_1975_017_013_02
11. Hutchings, I. M. The ricochet of spheres and cylinders from the surface of water. *Int. J. Mech. Sci.,* 1976, **18**, 241-7. doi: 10.1016/0020-7403(76)90006-0
12. Rayleigh, L. On the resistance of fluids. *Phil. Mag*., 1876, **2**(13), 430-441. doi: 10.1080/14786447608639132
13. Farouk, B.; Bassindowa, H. & Segletes, S. B. Impact and ricochet of a high-speed rigid projectile from an air-water interface. *Int. J. Multiphysics,* 2019, **13**, 157-77. doi: 10.21152/1750-9548.13.2.157
14. LSTC. LS-DYNA Theory Manual. 77-91, 2016
15. LSTC. LS-DYNA Keyword Users Manual, Version 971, Livermore Software Technology Corporation, Livermore CA. 2015.
16. Lowe, R. L.; Seidt, J. D. & Gilat, A. Characterization of the Lode = -1 meridian on the Al-2024 failure surface for *MAT_224 in LS-DYNA®. 14th Int. LS-DYNA Users Conference, 2016.
17. Segletes, S. B. A Rod Ricochet Model, ARL-TR-3257. Army Research Laboratory. 1 - 56, 2004. doi: 10.21236/ADA426125
18. Segletes, S. B. A model for rod ricochet. *Int. J. Impact Eng.,* 2006, **32**, 1403-39. doi: 10.1016/j.ijimpeng.2004.12.003
19. Segletes, S. B. Further development of a model for rod ricochet. *Int. J. Impact Eng*., 2007, **34**, 899-925. doi: 10.1016/j.ijimpeng.2006.03.004
20. Tate, A. A theory for the deceleration of long rods after impact. *J. Mech. Phy. Solids*, 1967, **15**, 387-99. doi: 10.1016/0022-5096(67)90010-5
21. Segletes, S. B. An adaptation of Walker-Anderson model elements into the Frank-Zook penetration model for use in MUVES. Tech. Report ARL-TR-2336, Army Research Laboratory (US), Aberdeen Proving Ground (MD), 2000. doi: 10.21236/ADA390872
22. http://asm.matweb.com/search/SpecificMaterial.asp?bassnum=MA2024T4.Aluminum 2024-T4; 2024-T351. (Accessed on 4 October 2021).
23. http://asm.matweb.com/search/SpecificMaterial.asp?bassnum=MTP641.Titanium Ti-6Al-4V (grade 5), annealed. (Accessed on 4 October 2021).

CONTRIBUTORS

Mr Hussein Bassindowa, received his MS from Drexel University, Philadelphia, PA where he is currently pursuing his PhD in the department of Mechanical Engineering and Mechanics. His area of interests are within the thermal fluid mechanical engineering field and he is currently researching fluid solid interactions (FSI) which includes sloshing, ricochet, and high speed flows over objects.
In the present study, his contributions are in the design and executaion of the FEM analysis and in preparing the numerous figures in the paper.

Dr Bakhtier Farouk, received his MS and PhD in Mechanical Engineering from the University of Delaware, Newark, DE in 1978 and 1981 respectively. His research and teaching interests include thermoacoustics, convective and radiative heat transfer, cryogenic refrigeration, plasma processing, combustion and fires, transport processes in materials processing, multi-phase flows, microfluidics, and computational fluid dynamics.
In the present study, he contributed by provoding overall guidance to the project and the development of the FEM models at the early statge.

Dr Steven B. Segletes, received MS in Mechanical Engineering and Mechanics from Drexel University, Philadelphia, Pennsylvania in 1984. He obtained in PhD from Drexel in 1988. He spent his career since 1980 working for the US Army at Aberdeen Proving Ground, Maryland, first at the US Army Ballistic Research Laboratory (BRL) and then at the US Army Research Laboratory (ARL). His research covers technology areas of direct relevance to the analysis of Army combat systems, including warhead mechanics, penetration mechanics, computational solid mechanics, condensed matter physics, thermodynamics, and explosive/metal interaction.
In the present study, he exercised his analytical model for rod ricochet to predict the ricochet outcome of the various scenarios that were simulated by his coauthors.